

PIPNet3D: Interpretable Detection of Alzheimer in MRI Scans

Lisa Anita De Santi^{1,6}, Jörg Schlötterer^{2,3}, Michael Scheschenja⁴, Joel Wessendorf⁴, Meike Nauta⁵, Vincenzo Positano⁶, Christin Seifert²

¹ University of Pisa, Pisa, Italy

² University of Marburg, Marburg, Germany

³ University of Mannheim, Mannheim, Germany

⁴ Department of Diagnostic and Interventional Radiology, University Hospital Marburg, Marburg, Germany

⁵ Datacation, Eindhoven, Netherlands

⁶ Fondazione Toscana G Monasterio, Pisa, Italy

Abstract. Information from neuroimaging examinations (CT, MRI) is increasingly used to support diagnoses of dementia, e.g., Alzheimer’s disease. While current clinical practice is mainly based on visual inspection and feature engineering, Deep Learning approaches can be used to automate the analysis and to discover new image-biomarkers. Part-prototype neural networks (PP-NN) are an alternative to standard blackbox models, and have shown promising results in general computer vision. PP-NN’s base their reasoning on prototypical image regions that are learned fully unsupervised, and combined with a simple-to-understand decision layer. We present PIPNet3D, a PP-NN for volumetric images. We apply PIPNet3D to the clinical case study of Alzheimer’s Disease diagnosis from structural Magnetic Resonance Imaging (sMRI). We assess the quality of prototypes under a systematic evaluation framework, propose new metrics to evaluate brain prototypes and perform an evaluation with domain experts. Our results show that PIPNet3D is an interpretable, compact model for Alzheimer’s diagnosis with its reasoning well aligned to medical domain knowledge. Notably, PIPNet3D achieves the same accuracy as its blackbox counterpart; and removing the remaining clinically irrelevant prototypes from its decision process does not decrease predictive performance.

Keywords: Deep Learning · XAI · Explainable AI · Interpretable Deep Learning · Part-prototypes · MRI · Alzheimer

1 Introduction

Alzheimer’s Disease (AD) is an irreversible neurodegenerative disease resulting in a progressive decline of cognitive abilities.

The diagnosis of AD is typically integrated with neuroimaging examinations, e.g., structural Magnetic Resonance Imaging (sMRI) [3,1,20]. Dementia patients exhibited pathological patterns in sMRI, such as gray matter atrophy and other

tissue abnormalities in specific brain areas [1]. There are no universally accepted methods to quantitatively analyze sMRI [1,20]. Deep Learning (DL) models can facilitate the analysis of imaging data and have the potential to extract yet unknown image-based biomarkers. However, the blackbox nature of DL models makes their application in high-stakes decisions controversial. Explainable Artificial Intelligence (XAI) aims to develop transparent systems while maintaining the advantages of DL [19,15,17]. For the application of XAI models in real-world scenarios, objectively assessing the quality of explanations is crucial [7]. As posthoc XAI approaches may not faithfully reflect a model’s reasoning [15], there is growing interest in self-explanatory models, where the model itself inherently provides the explanation. One such type of models are part-prototype neural networks (PP-NN), which base their reasoning on the detection of machine-learned *prototypical parts* [2]. Several works applied DL for AD diagnosis [4] from sMRI. While the majority use blackbox models, a few also applied PP-NN [9,10]. However, their models can not consider spatial relationships in the 3rd dimension [9], or use non-interpretable (nonlinear) decision layers [10].

There is an increasing interest in extending PP-NN models from general computer vision tasks to 3D medical images [2,22,21]. However, those works are based on ProtoPNet, which has been shown to lack in compactness of the explanation [16] and semantic quality of prototypes [12]. Among PP-NN models, PIPNet reported appealing properties for the medical domain [11], because it learns a small number of semantically meaningful prototypes, enables human interaction and direct manual adaptation of the model’s reasoning, and detects out-of-distribution data, abstaining from decisions when there is not sufficient evidence for any of the classes. As PIP-Net was designed for 2D images, and processing 3D volumes with a 2D backbone might induce information loss, we introduce PIPNet3D: an interpretable classifier able to process 3D scans.

In summary, our contributions are the following: (1) We introduce PIPNet3D, an interpretable-by-design part-prototype classifier for 3D input data, which is based on the PIPNet 2D model [12]. (2) We apply PIPNet3D to the clinical case study of AD diagnosis from sMRI, and find that PIPNet3D performs equally well to its corresponding blackbox baseline. (3) We thoroughly assess PIPNet3D w.r.t. comprehensive explanation desiderata and propose *Prototype Brain Entropy* and *Prototype Localization Consistency* as novel measures for functionally grounded evaluations. (4) We evaluate prototypes with two domain experts, and find that i) PIPNet3D aligns well with domain knowledge and ii) removing clinically irrelevant prototypes improved the model’s compactness without impacting classification performances. Source code and trained models are available at <https://anonymous.4open.science/r/PIPNet3D-58CA>.

2 Methodology

This section introduces the architecture of PIPNet3D (cf. Sect.2.1 and Fig. 1), which enables an understandable decision structure of the model (cf. Fig. 2). We

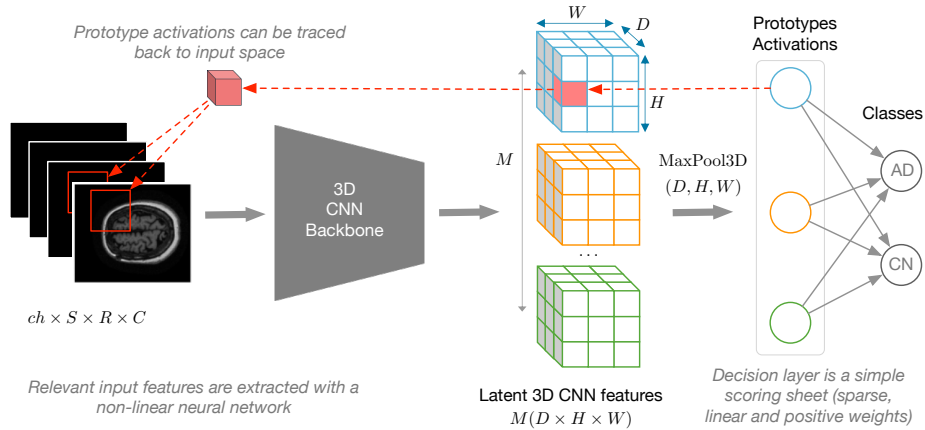


Fig. 1. Overview of PiPNet3D. 3D prototypes are learned through a CNN backbone. Representations are optimized through a contrastive pre-training step. A linear sparse decision layer computes the predictions based on prototype (VOI) activations.

describe the evaluation, including the novel metrics *Prototype Brain Entropy* and the *Prototypes Localization Consistency*, and expert evaluation in Sect. 2.2.

2.1 PIPNet3D

We designed our PIPNet3D based on a 3D-CNN feature extractor and follow the scoring-sheet reasoning and training paradigm of Nauta et al. [12]. The architecture (cf. Fig. 1) consists of an input layer, a CNN backbone, global max pooling of the feature maps, and a linear classification layer.

The **input layer** is of dimension $\mathbf{x} \in \mathbf{R}^{ch \times S \times R \times C}$ where ch, S, R, C respectively represents the number of channels, slices, rows and columns which constitutes the input volume. The **CNN backbone**, $z = f(\mathbf{x})$ extracts the latent features consisting of M 3-dim ($D \times H \times W$) feature maps where $z_{m,d,h,w}$ represents to the one-hot encoding of patch d, h, w to the prototype m . A **global max-pooling 3D** operation extracts M prototypes and calculates the prototypes presence scores \mathbf{p} where $p \in [0., 1.]^M$ and p_j measures the presence of the prototype m in the input image. The **linear classification layer** of size $\mathbf{w}_c \in \mathbf{R}_{>0}^{M \times K}$ connects prototypes to the classes acting as a scoring sheet, where $w_c^{m,k}$ represents the contribution of prototype m for class k . In our use case $k = 2$ classes: AD (Alzheimer’s disease) and CN (Cognitively Normal). This layer is optimized to be sparse (i.e., having as few connections as possible). The final output is a score for each of the K classes, where every **class output score** is given by the sum of the prototypes’ presence score weighted by the relevance of each prototype to that class: $\mathbf{o} = \mathbf{p} \cdot \mathbf{w}_c$, where \mathbf{o} is $1 \times K$ and $o_k = \sum_{d=1}^D p_d w_c^{d,k}$.

We selected ResNet18-3D [18] as backbone, which had been pre-trained on Kinetics400 data. This results in $M = 512$ prototypes.⁷ We applied data augmentation that do not alter the information content relevant to the clinical task [4] and trained PIPNet3D re-using the hyperparameter settings of the original PIPNet [12]. We only changed the batch size = 12 to adapt it to our computational capabilities. We reported the details on the data augmentation pipeline and hyperparameter setting in Suppl. Material.

After training, we selected the relevant prototypes, i.e., those that have a weight connection $w_c > 10^{-3}$ for at least one class and were detected with a similarity $p > 0.1$ in the training set [12]. The global explanation (cf. Fig. 2) consists of relevant prototypes of the most similar images in the training set marked as a volume of interest (VOI). During inference, PIPNet3D returns the predicted class and the annotation of every prototype detected in the image with similarity $p > 0.1$, together with its similarity score.

2.2 Neuroimaging Prototypes Explanation Quality

We assessed the explainability using the Co-12 evaluation framework [14,13] (details in Suppl. Material). We designed an automated quantitative functionally-grounded evaluation setup, and additionally an evaluation setup with domain experts. For both setups we defined quantitative metrics to perform objective measurements relevant to the neuroimaging domain. We apply the evaluation to compare the quality of the prototypes from the 5 different folds (denoted as \mathbf{M}_x where x indicates the current fold) and to study their relationship with their diagnostic performance.

Functionally Grounded Evaluation. We measured the compactness of PIPNet3D by calculating the total number of prototypes (*Global size*), the average number of detected prototypes in a test image (*Local size*), and the *Sparsity* of the decision layer following previous work [11]. Additionally, we propose two quality measures for prototypes based on brain reference standards to anatomically localize and study the composition of the extracted prototypes.

We propose *Prototype Brain Entropy* H_p to measure prototype purity. We used the Cerebrum Atlas (CerebrA) corresponding to the ICBM2009c space to annotate the prototypes with the anatomical brain regions [8]. For every prototype p_i we selected the corresponding VOI_p in the atlas, counted the voxels of every brain region, and computed the Shannon Entropy $H(\cdot)$ over brain regions. A “pure” prototype focused on one specific brain area has an $H_p = 0$, while a higher value indicates the inclusion of multiple regions. An explanatory Figure is reported in Suppl. Material.

$$H_p = H(\text{CerebrA}_{VOI_p}) \quad (1)$$

⁷ We also investigated a 3D backbone pre-trained on medical images [6], which yielded lower classification performance (57% accuracy, 61% F1). Detailed results are reported in the Suppl. Material.

We propose *Prototypes Localization Consistency* to measure whether the same prototype is activated in similar brain regions. We generate the local explanations for every image img in the test set, and evaluate the coordinate center (cc) of the VOI representing each prototype p , $VOI_{cc,p}|img$. Next, we compute the average prototype’s cc $\overline{VOI}_{cc,p}$. We then compute the Euclidean distance between $VOI_{cc,p}|img$ and $\overline{VOI}_{cc,p}$ and normalize for the maximum linear dimension of the VOI (for a cubic VOI $l\sqrt{3}$, where l is the side of the cube). We define *Prototypes Localization Consistency*, LC_p of p by averaging over the test set. LC_p ranges between 0 – 1 where 0 expresses the maximum localization consistency of the prototype. A prototype consistently located ($LC_p \approx 0$) can be associated with a specific brain region in the ICBM2009c standard space.

$$LC_p = \sum_{img} \frac{\|VOI_{cc,p}|img - \overline{VOI}_{cc,p}\|^2}{l\sqrt{3}} \quad (2)$$

Evaluation with Experts. We collected quantitative and qualitative feedback on the prototypes from two radiologists at an European University Hospital.⁸

Our survey prompted the participants to assess the following statements.⁹ “The prototype is located in a brain region typically affected in AD.” (*Localization coherence*). “A prototype adding evidence to CN does not show pathological patterns, a prototype adding evidence to AD shows an abnormal pattern.” (*Pattern coherence*). “The prediction returned by the model based on the VOI is correct.” (*Classification coherence*). For each item we used a 6-point Likert scale (1: strongly disagree – 6: strongly agree). Additionally, we asked participants “Which clues in this VOI vote for or against each diagnosis?” (free text). The radiologists assessed 35 prototypes in total. Each prototype was shown as i) a montage of the most activated image in the training set with the prototype marked with a VOI; ii) a detailed view montage of the extracted VOI.

We assessed the inter-user agreement for each item using the Interclass Correlation Coefficient (ICC) [5]. We averaged the scores of the two radiologists for every prototype and binarized the scores considering a prototype with a score ≥ 3.5 as coherent. We finally evaluated the rate of coherent prototypes. Additionally, we tested a human-in-the-loop setting by suppressing the incoherent prototypes from the model (setting PIPNet_{EK} in Table 1).

3 Evaluation

Data used in the preparation of this article were obtained from the Alzheimer’s Disease Neuroimaging Initiative (ADNI) database¹⁰. The ADNI was launched in 2003 as a public-private partnership, led by Principal Investigator Michael W.

⁸ anonymized for review

⁹ We performed two pre-tests, and only report on the final survey design.

¹⁰ <https://adni.loni.usc.edu>

Table 1. Performance comparison between blackbox ResNet and interpretable PIPNet (5 folds, in percentages). PIPNet_{EK} are models after pruning prototypes that do not align with expert knowledge (cf. Sect.2.2). \emptyset : averaged over 5 folds, *: best.

	Accuracy	F1	Precision		Recall	
			CN	AD	CN	AD
ResNet	80 \pm 06	79 \pm 06	86 \pm 06	77 \pm 08	78 \pm 14	82 \pm 11
PIPNet	82 \pm 02	79 \pm 03	82 \pm 04	84 \pm 09	88 \pm 07	76 \pm 09
AFTER ALIGNING WITH EXPERT KNOWLEDGE						
PIPNet _{EK} ^{\emptyset}	82 \pm 02	78 \pm 05	82 \pm 06	85 \pm 09	88 \pm 07	74 \pm 12
PIPNet _{EK} [*]	85	83	88	81	84	86

Weiner, MD. The primary goal of ADNI has been to test whether serial magnetic resonance imaging (MRI), positron emission tomography (PET), other biological markers, and clinical and neuropsychological assessment can be combined to measure the progression of mild cognitive impairment (MCI) and early Alzheimer’s disease (AD).

Selecting the “ADNI1 Standardized Screening Data Collection for 1.5T scans” processed with Gradwarp, B1 non-uniformity, and N3 correction, we obtained 307 CN and 243 AD sMRI brain scans. Our data pre-processing pipeline is inspired by Mulyadi et al. [10], detailed in Suppl. Material.

We performed 5-fold cross-validation with patient-wise random splits. 20% of training images are used for validation. We compared PIPNet3D to a black-box ResNet18-3D model, which we fine-tuned with dynamic data augmentation using the same augmentation pipeline as for PIPNet3D. We report hyperparameter settings in Suppl. Material. We implemented PIP3DNet using PyTorch and MONAI¹¹. We trained our models on an Intel Core i7 5.1 MHz PC, 32 GB RAM, equipped with an NVIDIA RTX3090 GPU with 24 GB of embedded RAM. The overall training process took on average 1 hour and 25 minutes and 1 hour for PIPNet3D and ResNet18-3D, respectively.

3.1 Predictive Performance

We evaluated the classification performances using Accuracy, F1, Precision and Recall (cf. Table 1). Paired two-tailed T-tests, $\alpha = 0.05$ showed no significant differences in classification performance between all 5 folds, suggesting that PIPNet3D adds interpretability to ResNet18-3D without reducing classification performance. We report classification performance and interpretability of related work (which is not directly comparable due to different subsets of the ADNI dataset) in Suppl. Material.

¹¹ <https://monai.io>

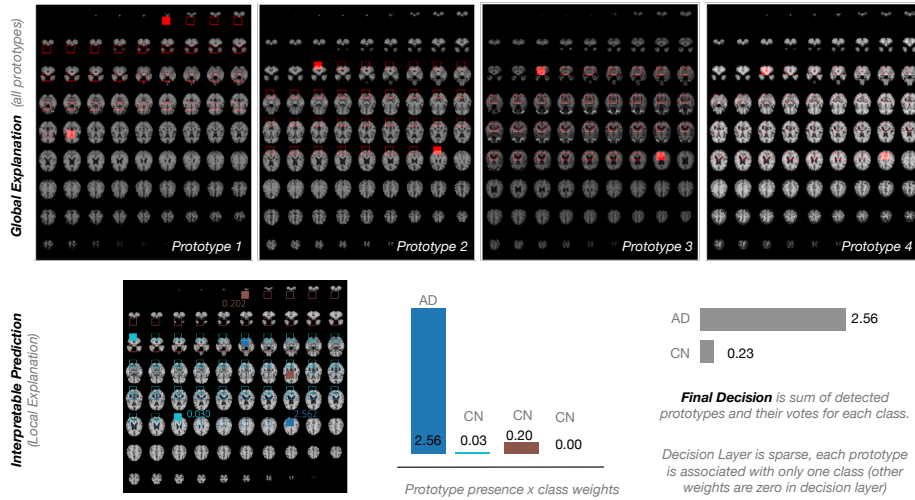


Fig. 2. Example of local and global explanation inherently provided by PIPNet3D (fold 5). The global explanation shows all prototypes of the models decision process. The local explanation shows the model’s reasoning for one particular patient.

3.2 Interpretability

Table 2 reports on the quality of prototypes. All folds of PIPNet3D have a small number of prototypes (Global size, max 11), while initially starting with a setup of 512 prototypes. Additionally, we observed that prototypes can uniquely be assigned to one class (e.g., the connection to the other class is zeroed out), leading to compact and comprehensible models.

Most of the prototypes are consistently located in the same anatomical location (small H_{p_i} , and LC_{p_i}). While all our models have a relatively small size (average 2.4 to 5.4 prototypes in local explanations), a Pearson correlation of 0.91 (± 0.03) between F1 score and Local size suggest that models with high accuracy are those with less compact local explanations (more prototypes). A Pearson correlation of $-0.89(\pm 0.04)$ between F1 and Prototype Entropy H_p , shows that a model with purer prototypes also has higher accuracy.

Our evaluation with domain experts showed a good reliability (ICC: 0.80, 0.76 and 0.85 for the quantitative tasks) [5]. Prototypes were found to be coherently located (coherence score 0.70, cf. Table 2), exhibit a coherent pattern (score 0.90), and classification decision (score 0.90). Most prototypes incoherently located are associated with the CN class (Localization coherence of 0.54, AD: 0.87). Incoherent CN prototypes might be due to PiPNet3D training scheme that requires finding evidence for every class; even if this class is representing absence of abnormalities.

We observed that most of the prototypes showed a coherent pattern with the connected class. This indicates that most of the prototypes provide evidence coherent with the medical knowledge to support the model’s decision. In this

Table 2. Evaluation of prototype quality for models M1, ..., M5. For the evaluation with experts, we show median rating in brackets. \uparrow and \downarrow : tendency for better values.

		M1	M2	M3	M4	M5	Average
FUNCTIONAL EVALUATION	Global size \downarrow	10	11	5	5	4	7.0
	for CN	5	4	3	3	3	3.6
	for AD	5	7	2	2	1	3.4
	Local size \downarrow	5.4	5.2	2.7	3.0	2.4	3.8
	Sparsity \uparrow	0.990	0.989	0.995	0.995	0.996	0.993
	LC_p \downarrow	0.004	0.021	0.008	0.018	0.030	0.016
	for CN	0.009	0.003	0.000	0.015	0.030	0.017
	for AD	0.000	0.016	0.020	0.022	0.050	0.022
	H_p \downarrow	2.5	3.1	3.4	3.1	3.4	3.1
	for CN	2.8	3.3	3.5	3.1	2.9	3.1
	for AD	2.3	2.9	3.3	3.1	3.8	3.1
	USERS	Localization Coherence \uparrow	0.90	0.60	0.60	0.80	0.50
for CN		0.80	0.25	0.67	0.67	0.33	0.54
for AD		1.00	0.86	0.50	1.00	1.00	0.87
Pattern Coherence \uparrow		1.00	0.90	0.80	0.80	0.80	0.90 (4.5)
for CN		1.00	1.00	1.00	1.00	0.67	0.93
for AD		1.00	0.86	0.50	0.50	1.00	0.77
Classification Coherence \uparrow		1.00	0.90	0.80	1.00	0.80	0.90 (4.5)
for CN		1.00	1.00	1.00	1.00	0.67	0.93
for AD		1.00	0.86	0.50	1.00	1.00	0.87

case, we observed a lower pattern coherence for the AD prototypes (0.77 vs. 0.93). We also noticed that most of the AD incoherent prototypes were observed in M3 and M4, where the model reported a lower recall for the AD class. We further analyzed the qualitative feedback for the prototypes that did not show a coherent pattern. For one CN prototype, both radiologists reported the presence of dilated ventricles as a viable sign of AD, suggesting incorrect model reasoning. For two AD prototypes, the VOI showed no or only mild pathological clues according to the radiologists. This may again point to incorrect model reasoning or indicate yet unknown patterns, that may not be visible to a human observer. We suppressed the prototypes that did not show a coherent pattern and we did not observe statistically significant differences in classification performance in the adapted models w.r.t. the original ones (cf. Table 1, models PIPNet_{EK}). Thus, adapting to domain knowledge increased the models’ compactness and coherency, without negatively impacting their accuracy.

4 Conclusion

In summary, we introduced PIPNet3D, a part-prototype model for 3D input images, applied to diagnose AD from sMRI, whose interpretability has been systematically assessed. We obtained an interpretable and compact model able to

support Alzheimer’s diagnosis with prototypes in line with medical knowledge. Our results show, that interpretable models that align with domain-knowledge can be as effective as blackbox models. We hope to inspire their usage in the future, especially in high-risk domains, such as medical image analysis. We plan to extend PIPNet3D to a multi-modal system additionally taking patients’ demographic information as input, and to increase the number of predicted classes by introducing intermediate levels of cognitive impairments. We also plan to design experiments to evaluate OoD performances with intermediate levels of dementia and patients with different age groups.

References

1. Chandra, A., Dervenoulas, G., Politis, M.: Magnetic resonance imaging in Alzheimer’s disease and mild cognitive impairment (6 2019). <https://doi.org/10.1007/s00415-018-9016-3>
2. Chen, C., Li, O., Tao, C., Barnett, A.J., Su, J., Rudin, C.: This looks like that: deep learning for interpretable image recognition. In: Proceedings of the 33rd International Conference on Neural Information Processing Systems. Curran Associates Inc., Red Hook, NY, USA (2019)
3. De Santi, L., Pasini, E., Santarelli, M., Genovesi, D., Positano, V.: An Explainable Convolutional Neural Network for the Early Diagnosis of Alzheimer’s Disease from 18F-FDG PET. *Journal of Digital Imaging* **36** (2023). <https://doi.org/10.1007/s10278-022-00719-3>
4. Khojaste-Sarakhshi, M., Haghighi, S.S., Ghomi, S.F., Marchiori, E.: Deep learning for Alzheimer’s disease diagnosis: A survey. *Artificial Intelligence in Medicine* **130**, 102332 (2022). <https://doi.org/https://doi.org/10.1016/j.artmed.2022.102332>
5. Koo, T.K., Li, M.Y.: A guideline of selecting and reporting intraclass correlation coefficients for reliability research. *Journal of Chiropractic Medicine* **15**(2), 155–163 (2016). <https://doi.org/https://doi.org/10.1016/j.jcm.2016.02.012>, <https://www.sciencedirect.com/science/article/pii/S1556370716000158>
6. Lee, H.H., Bao, S., Huo, Y., Landman, B.A.: 3d ux-net: A large kernel volumetric convnet modernizing hierarchical transformer for medical image segmentation. arXiv preprint arXiv:2209.15076 (2022)
7. Longo, L., Brcic, M., Cabitza, F., Choi, J., Confalonieri, R., Ser, J.D., Guidotti, R., Hayashi, Y., Herrera, F., Holzinger, A., Jiang, R., Khosravi, H., Lecue, F., Malgieri, G., Páez, A., Samek, W., Schneider, J., Speith, T., Stumpf, S.: Explainable Artificial Intelligence (XAI) 2.0: A manifesto of open challenges and interdisciplinary research directions. *Information Fusion* **106**, 102301 (2024). <https://doi.org/10.1016/j.inffus.2024.102301>
8. Manera, A.L., Dadar, M., Fonov, V., Collins, D.L.: Cerebra, registration and manual label correction of mindboggle-101 atlas for mni-icbm152 template. *Scientific Data* **7** (12 2020). <https://doi.org/10.1038/s41597-020-0557-9>
9. Mohammadjafari, S., Cevik, M., Thanabalasingam, M., Basar, A., Alzheimer’s Disease Neuroimaging Initiative: Using ProtoPNet for Interpretable Alzheimer’s Disease Classification. Canadian Artificial Intelligence Association (CAIAC) (2021)
10. Mulyadi, A.W., Jung, W., Oh, K., Yoon, J.S., Lee, K.H., Suk, H.I.: Estimating explainable Alzheimer’s disease likelihood map via clinically-guided prototype learning. *NeuroImage* **273** (6 2023). <https://doi.org/10.1016/j.neuroimage.2023.120073>
11. Nauta, M., Hegeman, J.H., Geerdink, J., Schlötterer, J., van Keulen, M., Seifert, C.: Interpreting and Correcting Medical Image Classification with PIP-Net. In: ECAI International Workshop on Explainable and Interpretable Machine Learning (XIML). pp. 198–215. Springer Nature Switzerland, Cham (2023). https://doi.org/10.1007/978-3-031-50396-2_11
12. Nauta, M., Schlötterer, J., van Keulen, M., Seifert, C.: PIP-Net: Patch-Based Intuitive Prototypes for Interpretable Image Classification. In: IEEE/CVF Conference on Computer Vision and Pattern Recognition (CVPR) (2023). <https://doi.org/10.1109/CVPR52729.2023.00269>
13. Nauta, M., Seifert, C.: The Co-12 Recipe for Evaluating Interpretable Part-Prototype Image Classifiers. In: Longo, L. (ed.) Proc. World Conference Explainable Artificial Intelligence (XAI). pp. 397–420. Springer Nature Switzerland, Cham (2023). <https://doi.org/https://arxiv.org/abs/2307.14517>

14. Nauta, M., Trienes, J., Pathak, S., Nguyen, E., Peters, M., Schmitt, Y., Schlötterer, J., van Keulen, M., Seifert, C.: From Anecdotal Evidence to Quantitative Evaluation Methods: A Systematic Review on Evaluating Explainable AI. *ACM Computing Surveys* (12 2023). <https://doi.org/10.1145/3583558>
15. Rudin, C.: Stop explaining black box machine learning models for high stakes decisions and use interpretable models instead. *Nature Machine Intelligence* **1**, 206–215 (5 2019). <https://doi.org/10.1038/s42256-019-0048-x>
16. Rymarczyk, D., Struski, Ł., Górszczak, M., Lewandowska, K., Tabor, J., Zieliński, B.: Interpretable image classification with differentiable prototypes assignment. In: *European Conference on Computer Vision*. pp. 351–368. Springer (2022)
17. Salahuddin, Z., Woodruff, H.C., Chatterjee, A., Lambin, P.: Transparency of deep neural networks for medical image analysis: A review of interpretability methods. *Computers in Biology and Medicine* **140**, 105111 (2022). <https://doi.org/10.1016/j.compbimed.2021.105111>
18. Tran, D., Wang, H., Torresani, L., Ray, J., LeCun, Y., Paluri, M.: A closer look at spatiotemporal convolutions for action recognition (11 2017), <http://arxiv.org/abs/1711.11248>
19. van der Velden, B.H., Kuijf, H.J., Gilhuijs, K.G., Viergever, M.A.: Explainable artificial intelligence (XAI) in deep learning-based medical image analysis, *Journal = Medical Image Analysis* **79**, 102470 (2022). <https://doi.org/https://doi.org/10.1016/j.media.2022.102470>
20. Vemuri, P., Jack, C.: Role of structural MRI in Alzheimer’s disease. *Alzheimer’s Research and Therapy* **2**(4) (2010). <https://doi.org/10.1186/alzrt47>
21. Wei, Y., Tam, R., Tang, X.: MProtonet: A case-based interpretable model for brain tumor classification with 3d multi-parametric magnetic resonance imaging. In: Oguz, I., Noble, J., Li, X., Styner, M., Baumgartner, C., Rusu, M., Heinmann, T., Kontos, D., Landman, B., Dawant, B. (eds.) *Medical Imaging with Deep Learning*. Proceedings of Machine Learning Research, vol. 227, pp. 1798–1812. PMLR (10–12 Jul 2024), <https://proceedings.mlr.press/v227/wei24a.html>
22. Wolf, T.N., Pölsterl, S., Wachinger, C.: Don’t PANIC: Prototypical Additive Neural Network for Interpretable Classification Alzheimer’s Disease. In: *Proceedings International Conference on Information Processing in Medical Imaging*. p. 82–94. Springer, Berlin, Heidelberg (2023). https://doi.org/10.1007/978-3-031-34048-2_7

PIPNet3D: Interpretable Detection of Alzheimer in MRI Scans

Classification Results - Alternative Backbone

Table 1: Performance over 5 folds. Showing percentages.

	Accuracy	F1	Precision		Recall	
			CN	AD	CN	AD
PIPNet _{UXNet}	57 ± 06	61 ± 02	70 ± 03	52 ± 06	50 ± 15	61 ± 02

Image Preprocessing: (1) Image registration to the ICBM152 Non-Linear Symmetric 2009c standard space ? with affine registration using SimpleITK ?. (2) Gray matter selection with the ICBM152 Non-Linear Symmetric 2009c brain mask. (3) Empty slices removal along the transverse axes (margin = 3 to the brain mask), 2 downsampling (reduce data dimensionality and speed up computation), final image size: $80 \times 114 \times 96$. (4) Min-max Intensity normalization to the range $[0 - 1]$.

Data Augmentation: Random rotation $\pm 10^\circ$ along x, y, z; random shift ± 5 along x, y, z; random zoom 0.9–1.1 and random Gaussian noise $N(0, 0.01)$. We finally repeated the channel to 3 to match the ResNet18-3D expected input dimension.

Table 2: **Hyperparameter settings.** PIPNet3D trained re-using the hyperparameters setting from the original paper ? and adapted batch size to our computational capabilities. ResNet18-3D trained re-using hyperparameters setting from ? which implemented the ResNet18-3D architecture in the work) and adapted batch size (same batch size of PIPNet3D)

PIPNet3D	ResNet18-3D
(1) Self-Supervised learning of prototypes: Adam optimizer, backbone learning rate 0.0001, linear classification learning rate 0 (frozen), batch size 12, 10 epochs;	Adam optimizer, learning rate 10^{-4} , batch size 24, 100 epochs .
(2) PIPNet training: Adam optimizer, backbone learning rate 0.0001, linear classification learning rate 0.05, batch size 12, 60 epochs.	

Relevant Work

Table 3: Classification performances (F1) and model’s interpretability of related work

Authors	F1	Models and Interpretability
?	0.88	ResNet18-3D with Attention Mechanism producing explanation heatmaps
?	0.88	Adapted 3D VoxCNN and ResNet with posthoc explanation heatmaps
?	0.89	3D CNN with posthoc explanation heatmaps and t-SNE
?	0.91	ResNet18-3D with Prototypical Latent Space classified by a NN
Ours	0.79	3D ResNet-18 baseline black-box model
	0.79	PiPNet3D: Interpretable-by-design PP model

arXiv:2403.18328v1 [cs.CV] 27 Mar 2024

Table 4: The Co-12 assessment of PIPNet’s interpretability

Criterion		
CONTENT	Correctness	Classification correct by design. Visualization with upsampling ? might not be fully correct ?, and is direction of future work.
	Completeness	Complete by design; the full model behavior (linear layer connections is explained). Representation learning (backbone) as blackbox with interpretable output (prototypes).
	Consistency	Consistent by design (no random components in the forward pass computations), but may be subject to standard numerical computation differences. We assessed the difference in prototype’s localization when detected in different subjects (cf. LC_p).
	Continuity	Optimized by the contrastive learning setup of PIPNet, but not explicitly evaluated.
	Contrastivity	Output-sensitivity implemented by-design.
	Cov. complexity	Prototype purity assessed with anatomical brain atlas annotation (cf. H_p).
PRESENTATION	Compactness	Evaluated by <i>global</i> and <i>local explanation size</i> .
	Composition	Showing both, overview and detail; localization of the found prototype in the brain, and its detail view.
	Confidence	Diagnosis prediction reported together with the prototypes’ similarity score which constitutes the Alzheimer’s fingerprint of the subject and the OoD detection confidence.
USER	Context	We evaluated prototypes with domain experts in a human-grounded evaluation.
	Coherence	User study with radiologists evaluating whether the prototypes align with experts’ visual assessment w.r.t. their localization, detected pattern, and diagnostic decision (cf. <i>Localization Coherence</i> , <i>Pattern Coherence</i> , <i>Classification Coherence</i>).
	Controllability	We use results collected from the coherence analysis to suppress the prototypes that are not in line with the expert evaluation.

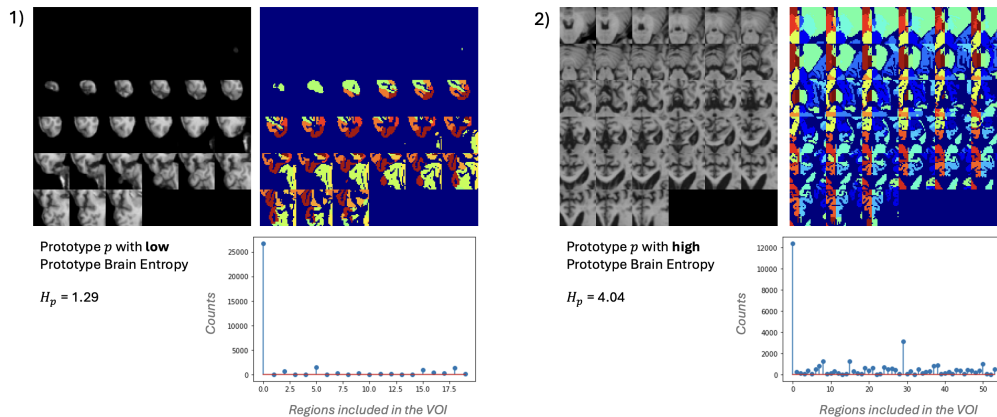


Figure 1: Montage of the image VOI, VOI in the CerebrA atlas, and counts of the CerebrA regions in the VOI for two different prototypes. 1) represent a “pure” prototype (lower H_p); 2) represent an “impure” prototype (higher H_p)